JOURNAL OF MATERIALS SCIENCE 31 (1996) 262–266

Porosity-dependence of elastic properties and ultrasonic velocity in polycrystalline alumina – a model based on cylindrical pores

K. K. PHANI
Central Glass and Ceramic Research Institute, Calcutta 700 032, India

Effective elastic moduli and ultrasonic velocity of materials having aligned cylindrical pores have been derived using a series expansion in terms of the difference between the upper and lower bounds of elastic moduli obtained by the variational method. The theoretical results for polycrystalline alumina agree well with the experimental data, confirming the suggestion of previous researchers that a matrix containing parallel cylindrical pores orientated perpendicular to the applied stress, provide a better model than a spherical one in describing the porosity-dependence of elastic moduli in sintered specimens.

1. Introduction

Extensive experimental and theoretical work has been done to determine the effect of porosity on the elastic properties of ceramics. However, the theoretical results based on spherical porosity [1–4] show a large discrepancy with the experimentally observed effect of porosity on elastic moduli [5, 6]. Dean [7] was possibly the first researcher to provide a rigorous comparison between the theory and experiment, taking into account the non-spherical nature of the pores. He could explain the observed variation of elastic moduli with porosity for six cases out of seven selected data sets investigated, based on the self-consistent oblate spheroidal inclusion theory [8].

The present author [9] has also used the same theory to explain the observed variation of ultrasonic velocity with porosity. Out of ten cases investigated, the theory failed to explain the observed variation in two of the data sets, one of which was the data on polycrystalline alumina reported by Nagarajan [6]. The failure of the self-consistent oblate spheroidal theory in this case was attributed to the difference in the pore geometry of specimens and that assumed in the theory. From the analysis of his experimental data on elastic moduli, Nagarajan [6] concluded that a cylindrical pore model with the pores orientated perpendicular to the stress, described the data much better than a spherical one.

A similar conclusion was also drawn earlier by Hasselman and Fulrath [5] by comparing the data on alumina compiled by Knudsen [10], with the bounds of elastic moduli derived from Hashin and Rosen's [11] analysis of elastic properties of matrices containing arrays of parallel cylindrical fibres, by setting the elastic properties of the fibres identically equal to zero. They suggested that in sintered bodies at least part of the porosity might be cylindrical, especially at higher porosities, where the pores tended to be interconnected (open porosity), rather than isolated (closed or spherical). Thus a model based on cylindrical pores orientated perpendicular to the applied stress should provide a better explanation of the observed variation of elastic moduli with porosity, at least in the case of polycrystalline alumina data investigated.

The "elastic-bound" model of Hashin and Rosen [11] expresses the stress energy in terms of the elastic moduli and provides upper and lower bounds for them based on the variational principles of minimum potential energy and minimum complementary energy. For random arrangement of fibres in the transverse plane, their results are expressed in terms of a bulk modulus (for which upper and lower bound coincide) and upper and lower bounds for shear modulus. In the bounding approach, the variation of elastic moduli with porosity can be effectively predicted only if the upper and lower bounds are sufficiently close so as to bracket the true behaviour of the material within the experimental error inherent in elastic moduli measurements. Unfortunately, porous materials have bounds that are widely separated. This is because pores are filled with air which has negligible bulk modulus compared to that of the matrix. Thus the elastic bounds for porous material remain too far apart to serve the purpose of prediction of elastic properties within the margin of experimental error. A similar situation arises in the case of particulate composites, such as rubber-toughened polymers, where the inclusions are more compliant than the matrix. To overcome this problem, in the case of composite materials, a modelling approach based on series expansion in terms of the difference between the upper and lower bounds has been used to predict the effective properties of the material [12]. In this paper, the same approach is used to derive elastic moduli–porosity relations for materials with cylindrical pores using the bounds given by Hashin and

0022–2461

Rosen [11]. Theoretical results are also compared with the data on polycrystalline alumina reported by Knudsen [10] and Nagarajan [6].

2. Theoretical derivations

The introduction of parallel cylindrical pores into a matrix results in considerable elastic anisotropy. For random arrangement of pores in the transverse plane, the material is assumed to be transversely isotropic [11]. Considering a Cartesian-coordinate system 123 with the 1-axis in the pore direction and the 2,3-axes in the transverse plane, and setting the elastic properties of the fibres identically equal to zero, Hashin and Rosen's [11] bounds of effective elastic moduli in the 23-plane are given by

$$K_{23}^{*} = \frac{2(K_0 + G_0/3)\nu_0(1-\phi)}{2\nu_0 + \phi} \tag{1}$$

$$G_{23}^{*(+)} = G_0\left[1 - \frac{2(1-\nu_0)}{1-2\nu_0}\phi A^{\varepsilon}\right] \tag{2}$$

$$G_{23}^{*(-)} = G_0\Big/\left[1 + \frac{2(1-\nu_0)}{1-2\nu_0}\phi A^{\sigma}\right] \tag{3}$$

where ϕ is the volume fraction of pores, K, G and ν are the bulk modulus, shear modulus and Poisson's ratio, respectively. The subscript 0 refers to a pore-free i.e. theoretically dense material and the superscript *, + and − signs indicate the effective modulus, upper and lower bounds, respectively. The values of A^{ε} and A^{σ} are obtained by solving a system of linear equations (Equations 109–119 in [11]) and are given by

$$A^{\varepsilon} = \frac{2(1-2\nu_0)[(4\nu_0 - 3) - \phi^3]}{4\nu_0(\phi^4 + 6\phi - 4\nu_0\phi + 1) - (3\phi^4 + 4\phi^3 - 6\phi^2 + 12\phi) - 3} \tag{4}$$

$$A^{\sigma} = \frac{2(1-2\nu_0)(1-\phi^3)}{(\phi^4 - 4\phi^3 + 6\phi^2 - 4\phi + 1)} \tag{5}$$

For bulk modulus, the upper and lower bounds are coincident, but for shear modulus, they are different. The upper and lower bounds of the shear modulus for alumina are shown in Fig. 1. As mentioned before, these bounds are not close enough to give any useful estimate of the effective shear modulus of the material. The material behaviour will tend toward the upper bound as ϕ approaches zero; on the other hand, as ϕ approaches unity, it will be closer to the lower bound. Thus the difference between the upper and lower bounds serves as a measure of the influence of the microgeometry coupled with the properties of the components. So it is reasonable to assume that the effective shear modulus may be modelled as a series expansion in terms of the difference between the upper and lower bounds [12]. Thus, retaining only the linear term, G_{23}^{*} is given by

$$G_{23}^{*} = G_{23}^{*(+)} - \psi(G_{23}^{*(+)} - G_{23}^{*(-)}) + \cdots \tag{6}$$

where ψ, a function of ϕ, is a proportionality factor. Because the effective modulus value must fall between the extremes of the upper and lower bounds, the term $\psi(\phi)$ must satisfy the condition $0 < \psi(\phi) < 1$.

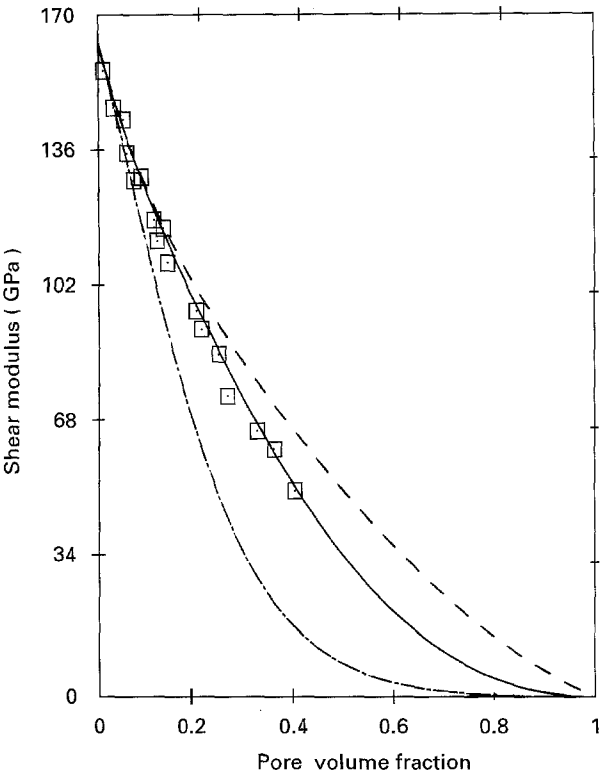

Figure 1 Calculated and observed effects of parallel cylindrical pores on the shear modulus of Al_2O_3 (data from [6]). (– – –) Upper bound, (— – —) lower bound, (——) present theory.

G_{23}^{*} should tend toward the upper bound as ϕ approaches 0; alternately, as ϕ approaches 1, G_{23}^{*} should tend to the lower bound. This condition can be assured by requiring that $\psi(0) = 0$ and $\psi(1) = 1$. Assuming that $\psi(\phi)$ can be adequately approximated by a truncated series expansion in ϕ, i.e.

$$\psi(\phi) = \alpha + \beta\phi + \gamma\phi^2 \tag{7}$$

the above two conditions give

$$\psi(0) = \alpha = 0 \tag{8}$$

$$\psi(1) = \alpha + \beta + \gamma \tag{9}$$

thus

$$\psi(\phi) = (1-\gamma)\phi + \gamma\phi^2 \tag{10}$$

Substituting Equation 10 into Equation 6

$$G_{23}^{*} = (1-\phi)(1+\gamma\phi)G_{23}^{*(+)} + \phi(1-\gamma+\gamma\phi)G_{23}^{*(-)} \tag{11}$$

The surviving parameter, γ, is evaluated by using the concept of "contiguity" described by Hashin [4], which is defined as the average fraction of surface area shared by a pore with all neighbouring pores. The contiguity will be an increasing function of the pore volume fraction and can be expected to be very small only in the case of low volume fraction of pores. Thus at low volume fraction of pores, the matrix will remain continuous and it is expected that the effective modulus will tend toward the upper limit of elastic modulus. On the other hand, with increase in contiguity for increasing pore volume, pores will become more and more interconnected and it is expected that the effective modulus will tend toward the lower limit. Now for a hexagonal close packing of pores of circular

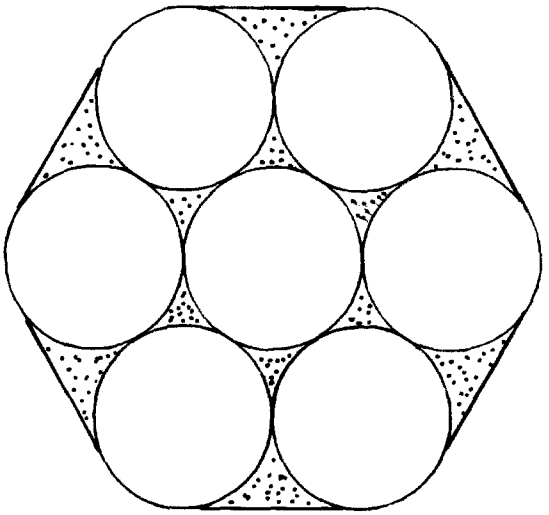

Figure 2 Hexagonal array of cylindrical pores.

cross-section as shown in Fig. 2, the maximum volume fraction that can be achieved is $\phi^{max} = (\pi/6)3^{1/2} = 0.9069$. Any value of $\phi > 0.9069$ would correspond to a continuous pore phase containing matrix inclusion. Alternatively, for a hypothetical system of equivalent cylindrical particles of matrix material embedded in a continuous "pore" phase, the maximum fraction of matrix in excess of 0.9069 would lower the porosity which is now given by $(1 - \phi^{max})$, making the matrix phase continuous. In the case of square array, a similar situation will arise for $\phi^{max} = \pi/4 = 0.7854$. In terms of the notion of "contiguity", the situation $\phi > \phi^{max}$ corresponds to "zero" matrix contiguity in the sense that the average contact area of neighbouring matrix zones is zero; the situation for $\phi < 1 - \phi^{max}$ corresponds to "zero" pore contiguity. Intermediate states of contiguity are obtained between these limits of pore volume fraction, i.e. $\phi^{max} < \phi < 1 - \phi^{max}$.

These considerations imply that at some critical pore volume fraction, ϕ_c, a transition in phase contiguity must occur so that in the neighbourhood of $\phi = \phi_c$, the behaviour tends toward the limits of the lower bound, while in the vicinity of $\phi = 1 - \phi_c$, the behaviour will tend toward the limits of the upper bound. For random distributions of pores it is assumed that the various packing forms mentioned earlier occur at random with equal probability and the value ϕ_c for such random packing is taken as the average of ϕ^{max} values of the above two forms, i.e. $\phi_c = 0.846$. Thus, assuming that as $\phi \to \phi_c + \delta\phi_c$, G_{23}^* is within ε of $G_{23}^{*(-)}$ and similarly as $\phi \to 1 - (\phi_c + \delta\phi_c)$, G_{23}^* will be within an equivalent range of $G_{23}^{*(+)}$, one gets

$$[G_{23}^*]_{\phi=\phi_c} = [G_{23}^{*(-)}]_{\phi=\phi_c} + \varepsilon \tag{12}$$

$$[G_{23}^*]_{\phi=1-\phi_c} = [G_{23}^{*(+)}]_{\phi=1-\phi_c} - \varepsilon \tag{13}$$

neglecting the small term $\delta\phi_c$. Using Equations 2, 3 and 11, these two equations can be solved to obtain the value of γ. The expression for γ is quite complex and is given in the Appendix. Once γ is known for a system, the value of G_{23}^* can be evaluated from Equation 11. Transverse Young's modulus, $E_2^* = E_3^*$ in the 23-plane can then be evaluated from the relations given by Hashin and Rosen [11], i.e.

$$E_2^* = E_3^* = \frac{4G_{23}^* K_{23}^*}{K_{23}^* + \xi G_{23}^*} \tag{14}$$

where

$$\xi = 1 + \frac{4K_{23}^* \nu_1^{*2}}{E_1^*} \tag{15}$$

Young's modulus, E_1^*, parallel to the pores follows the law of mixtures and is given by

$$E_1^* = E_0(1 - \phi) \tag{16}$$

ν_1^*, the longitudinal Poisson's ratio, is given by $\nu_1^* = \nu_0$. For propagation of an ultrasonic wave in the 2 or 3 direction, the longitudinal and transverse velocity values are given by

$$V_l = [(K_{23}^* + G_{23}^*)/\rho]^{1/2} \tag{17}$$

$$V_t = [G_{23}^*/\rho]^{1/2} \tag{18}$$

where the density, ρ, is calculated from the theoretically dense material, ρ_0, using the relation

$$\rho = \rho_0(1 - \phi) \tag{19}$$

A comparison of experimental data with the theory is given below.

3. Results and discussion

Experimental data of Young's modulus and shear modulus on Al_2O_3 by Nagarajan [6] are shown in Figs 1 and 3, respectively. A computer program was run to calculate the values of G_{23}^* and E_2^* from Equations 11 and 14. Mean polycrystalline (Voight, Reuss, Hill average) elastic moduli values for K_0 and G_0 reported by Anderson *et al.* [13] were used in the theoretical calculations. These values, $K_0 = 251.0$ and $G_0 = 162.9$ GPa, were obtained from the measured single-crystal elastic constants. The values of E_0 and ν_0 were taken as 402.0 GPa and 0.25, respectively. Equation A1 gave the value of $\gamma = 0.50$. The theoretical curves for G_{23}^* and E_2^* are shown in Figs 1 and 3, respectively. The upper and lower bounds for Young's modulus computed from Equation 14 using Equations 1–3 are also shown in Fig. 3. Fig. 1 speaks for itself in terms of the comparison between experiment and theory. However, in the case of Young's modulus (Fig. 3), the theory tends to overestimate the value slightly. This may be because of the fact that, whereas the expressions for bounds of shear modulus, i.e. Equations 2 and 3, are the exact results, the expression for bulk modulus, Equation 1, is an approximate one [11]. It may also be noted that Equation 1 fails to give $K_{23}^* = K_0$ at $\phi = 0$ due to anisotropy assumptions.

Fig. 4 shows the theoretical velocity values calculated from Equations 17 and 18 along with the experimental data reported by Nagarajan [6]. A value of $\rho_0 = 3.98\ \mathrm{gm\,cm^{-3}}$ was used in the calculation. Here, again, the fit between theory and experimental values for transverse velocity is almost as impressive as that of shear-modulus data. However, the theory overestimates the longitudinal velocity by about 10%, possibly because of the reasons mentioned earlier. But

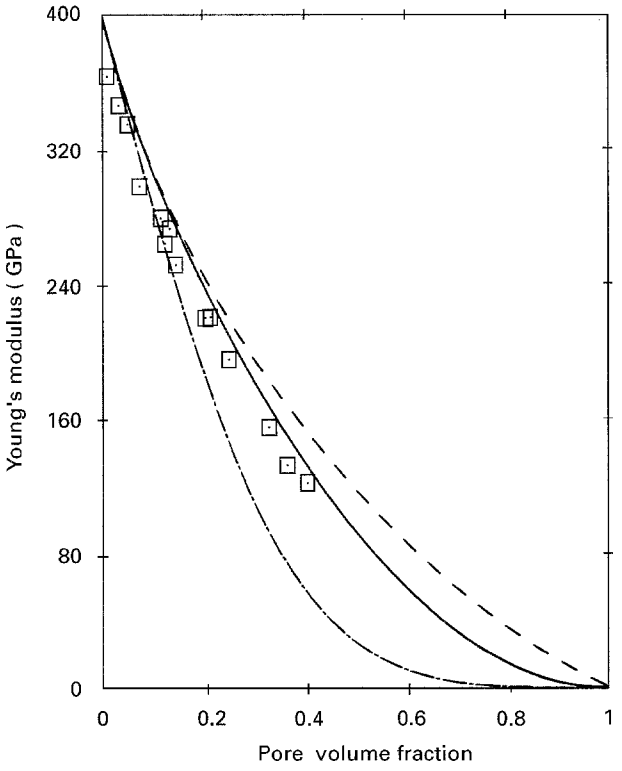

Figure 3 Calculated and observed effects of parallel cylindrical pores on Young's modulus of Al_2O_3 (data from [6]). (---) Upper bound, (— - —) lower bound, (——) present theory.

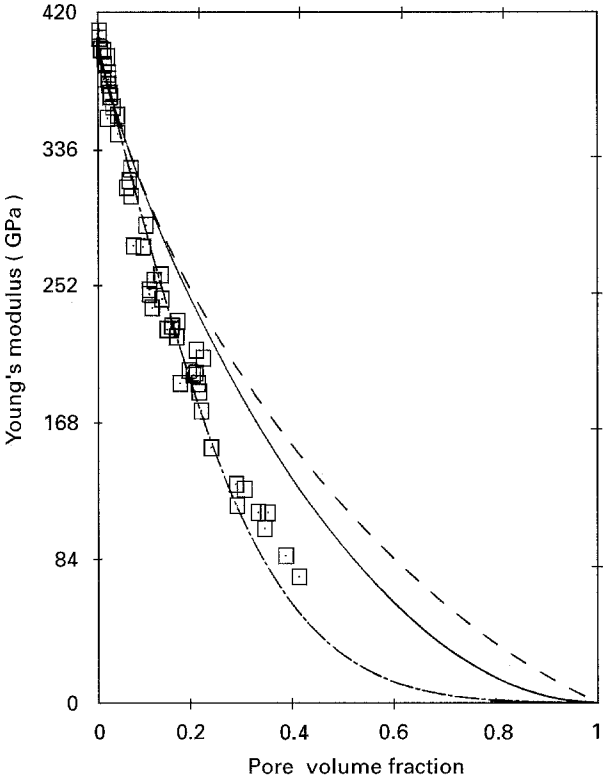

Figure 5 Calculated and observed effects of parallel cylindrical pores on the Young's modulus of Al_2O_3 (data from [10]). (---) Upper bound, (— - —) lower bound, (——) present theory.

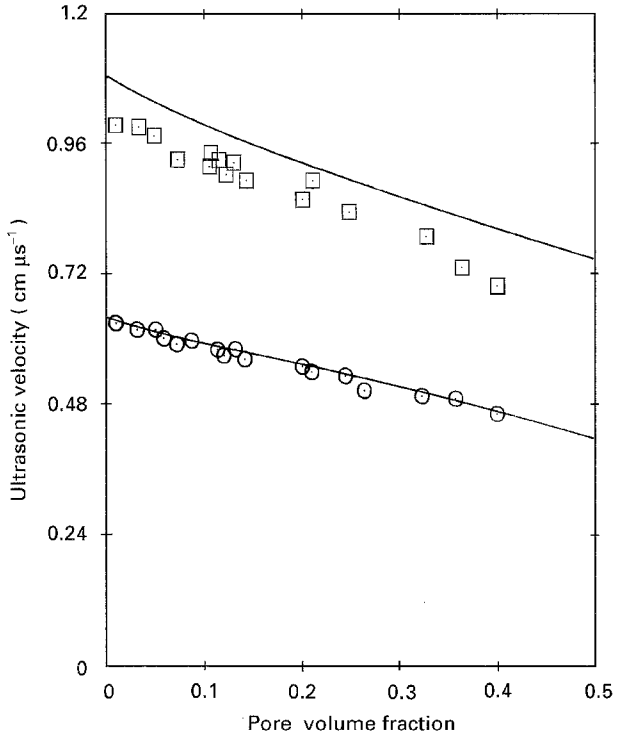

Figure 4 Calculated and observed effects of parallel cylindrical pores on the ultrasonic velocity of Al_2O_3 (data from [6]). ⊡ Longitudinal, ⊙ transverse.

the variation of the velocity with the porosity (the slope) is in good agreement with the theory.

It may be noted that ϕ_c was taken as 0.846 in the theoretical calculation. This shows that "zero" pore contiguity condition is achieved at a pore volume fraction of 0.154. Nagarajan's [6] data on porosity (Fig. 1 in [6]) show that when the total pore volume fraction is 0.154, only about 0.03 volume fraction is open pores. So the major portion of the pores are isolated, making the matrix phase continuous. Thus the elastic moduli should be close to the upper bound as per the assumption of the theory. The data shown in Figs 1 and 3 closely follow the upper bound curve confirming the validity of the assumption. On the other hand, "zero" matrix contiguity is assumed to be achieved at a pore volume fraction of 0.846. Nagarajan's [6] data (Fig. 1 in [6]) show that even at a pore volume fraction of 0.40, 80% of it can be accounted for by open pores (interconnected). Thus even at this level of porosity the effective moduli will tend towards the lower bound. This is again confirmed from the data shown in Figs 1 and 3, thus validating the assumption regarding the value of ϕ_c.

Fig. 5 compares the experimental data on alumina, as compiled by Knudsen [10] with the theoretical value. The figure shows that up to a porosity of about 15%, the data are in fair agreement with the theory, but above this porosity the data almost follow curve of lower bound of Young's modulus. This indicates that for this group of data, ϕ_c is possibly lower than that assumed in the deduction of the theory. However, no details about the pore structure are available to confirm this. It may also be noted that the data shown in Fig. 5 have been compiled from the work of different researchers whose methods of fabrication varied. Thus the assumption that different batches of materials have the same pore structure may not be strictly valid. This may also be the reason for the deviation of theory from the experiment.

4. Conclusion

The elastic moduli and ultrasonic velocity of materials having aligned cylindrical pores have been derived using a series expansion in terms of the difference between the upper and lower bounds of elastic moduli obtained by the variational method. The theoretical results for polycrystalline alumina agree well with the experimental data. Analysis shows that a matrix containing parallel cylindrical pores oriented perpendicular to the applied stress provide a better mechanical model than a matrix containing spherical pores for predicting the effect of porosity on elastic moduli and ultrasonic velocity at least in the case of the data on the alumina studied.

Acknowledgement

The author thanks Dr B. K. Sarkar, Director of the Institute for his permission to publish this paper.

Appendix

Solution of Equations 12 and 13 yields

$$\gamma = (F_1 + F_2)/(F_3 + F_4 + F_5 + F_6) \quad \text{(A1)}$$

where

$$F_1 = \phi_c(1 - \phi_c)[2 - b\phi_c(A^\varepsilon)_{\phi=\phi_c} - b(1 - \phi_c)(A^\varepsilon)_{\phi=1-\phi_c}] \quad \text{(A2)}$$

$$F_2 = \phi_c(\phi_c - 1)\{1/[1 + b\phi_c(A^\sigma)_{\phi=\phi_c} + 1/[1 + b(1 - \phi_c)(A^\sigma)_{\phi=1-\phi_c}]\} \quad \text{(A3)}$$

$$F_3 = 1/[1 + b\phi_c(A^\sigma)_{\phi=\phi_c}] + 1 - b(1 - \phi_c)(A^\varepsilon)_{\phi=1-\phi_c} \quad \text{(A4)}$$

$$F_4 = (\phi_c - 1)[1 - b\phi_c(A^\varepsilon)_{\phi=\phi_c}] \quad \text{(A5)}$$

$$F_5 = -\phi_c[1 - b(1 - \phi_c)(A^\varepsilon)_{\phi=1-\phi_c}] \quad \text{(A6)}$$

$$F_6 = -\{\phi_c/[1 + b\phi_c(A^\sigma)_{\phi=\phi_c}] + (1 - \phi_c)/[1 + b(1 - \phi_c)(A^\sigma)_{\phi=1-\phi_c}]\} \quad \text{(A7)}$$

$$b = 2(1 - \nu_0)/(1 - 2\nu_0) \quad \text{(A8)}$$

and $(A)^{\varepsilon \text{ or } \sigma}_{\phi=p}$ indicates that the value of the parameter A is evaluated for $\phi = p$.

References

1. J. M. DEWEY, *J. Appl. Phys.* **18** (1947) 578.
2. J. K. MACKENZIE, *Proc Phys. Soc. (Lond)* **B63** (1950) 2.
3. E. H. KERNER, *ibid.* **B69** (1956) 808.
4. Z. HASHIN, *J. Appl. Mech.* **29** (1962) 143.
5. D. P. H. HASSELMAN and R. M. FULRATH, *J. Am. Ceram. Soc.* **48** (1965) 545.
6. A. NAGARAJAN, *J. Appl. Phys.* **42** (1971) 3693.
7. E. A. DEAN, *J. Am. Ceram. Soc.* **66** (1983) 847.
8. T. T. WU, *Int. J. Solids Struct.* **3** (1966) 1.
9. K. K. PHANI, *J. Mater. Sci.* submitted.
10. F. P. KNUDSEN, *J. Am. Ceram. Soc.* **45** (1962) 94.
11. Z. HASHIN and B. W. ROSEN, *J. Appl. Mech.* **31** (1964) 223.
12. J. M. WHITNEY and R. L. MCCULLOUGH, in "Composite Design Guide", Vol. 2, D. W. Wilson, R. C. Wetherhold, H. M. Cadot, R. L. Mccullough and R. Byron Pipes (eds) (University of Delaware, DE, 1981) Section 2.4, p. 47.
13. O. L. ANDERSON, E. SCHREIBER, R. C. LIEBERMAN and N. SOGA, *Rev. Geophys.* **6** (1968) 491.

Received 8 December 1993
and accepted 7 June 1995